Structural and biochemical requirements for secretory component interactions with dimeric Immunoglobulin A

Sonya Kumar Bharathkar and Beth M. Stadtmueller[1,2,3*]

[1]Department of Biochemistry, University of Illinois Urbana-Champaign, Urbana, Illinois 61801 USA

[2]Department of Biomedical and Translational Sciences, Carle Illinois College of Medicine, University of Illinois Urbana-Champaign, Urbana, Illinois 61801 USA

[3]Carle R. Woese Institute of Genomic Biology

*Address correspondence to bethms@illinois.edu–

ABSTRACT

Secretory (S) Immunoglobulin (Ig) A is the predominant mucosal antibody that protects host epithelial barriers and promotes microbial homeostasis. SIgA production occurs when plasma cells assemble two copies of monomeric IgA and one joining chain (JC) to form dimeric (d) IgA, which is bound by the polymeric Ig receptor (pIgR) on the basolateral surface of epithelial cells and transcytosed to the apical surface. There, pIgR is proteolytically cleaved, releasing SIgA, a complex of the dIgA and the pIgR ectodomain, called secretory component (SC). The pIgR has five Ig-like domains (D1-D5) that undergo a conformational change upon binding dIgA, ultimately contacting four IgA heavy chains and the JC in SIgA. Here we report structure-based mutational analysis combined with surface plasmon resonance binding assays that identify key residues in mouse SC D1 and D3 that mediate SC binding to dIgA. Residues in D1 CDR3 are likely to initiate binding whereas residues that stabilize the D1-D3 interface are likely to promote the conformation change and stabilize the final SIgA structure. Additionally, we find that the three C-terminal residues of JC play a limited role in dIgA assembly but a significant role in pIgR/SC binding to dIgA. Together results inform new models for the intricate mechanisms underlying IgA transport across epithelia and functions in the mucosa.

INTRODUCTION

Secretory Immunoglobin A (SIgA) is a crucial antibody in the mucosal immune system that helps maintain the balance of microorganisms and protect the mucosal barrier (1),(2). The assembly of SIgA begins in the lamina propria, where plasma cells link one Joining chain (JC) and between two to five monomeric (m) IgA to form or polymeric (p) IgA; in humans the predominant form is dimeric (d) IgA(3),(4),(5). Subsequently, pIgA binds to polymeric Ig Receptor (pIgR) on the basolateral surface of mucosal epithelia and is then transcytosed to the apical side(6),(7). In the mucosa, proteases cleave the pIgR ectodomain from the cell surface, releasing a complex containing pIgR's five Ig-like domains (D1-D5), collectively referred to as Secretory Component (SC), bound to the pIgA(8),(9). The SC-pIgA complex, which typically includes dIgA, is referred to as SIgA(10).

Each mIgA consists of two heavy chains (HC) and two light chains (LC) that together form two antigen binding fragments (Fabs) and one constant fragment (Fcα), and thus SIgA contains at least four Fabs and two Fcs (Fig.1). The cryo-EM structures of SIgA(11),(12),(13) and dIgA(11) revealed a remarkably asymmetric molecule with individual mIgAs bent and tilted with respect to each other. This arrangement results in each HC (HC-A-D) adopting a unique structure and unique contacts with other chains, despite sharing the same sequence. The greatest structural variability is found among copies of the HC's 18-22 residue C-terminal extension, called the tailpiece (Tp) (11),(12),(13). The four Tps (TpA-D) co-fold with JC to form a β-sandwich, in which the Tps closest to JC, TpA and TpC, are disulfide bonded to the JC with their penultimate Cys residue(11),(12),(13),(14). The other two Tps, TpB and TpD, are partially disordered in dIgA, but are ordered in SIgA, indicating a possible role in pIgR binding and successful SIgA formation(11). In addition to contacting the Tps, the JC also contacts HC residues in the Fcα regions, through several β-hairpins, termed *wings*. JC_{wing-1} and JC_{wing-2} contact HC-C and HC-A respectively, and appear to contribute to the bent, asymmetric conformation observed for both dIgA and SIgA. Additionally JC also contacts parts of SC with its C-terminal residues interfacing with SC-D1, and JC_{wing-1} interfacing with SC-D4-D5 (11),(12),(13).

52

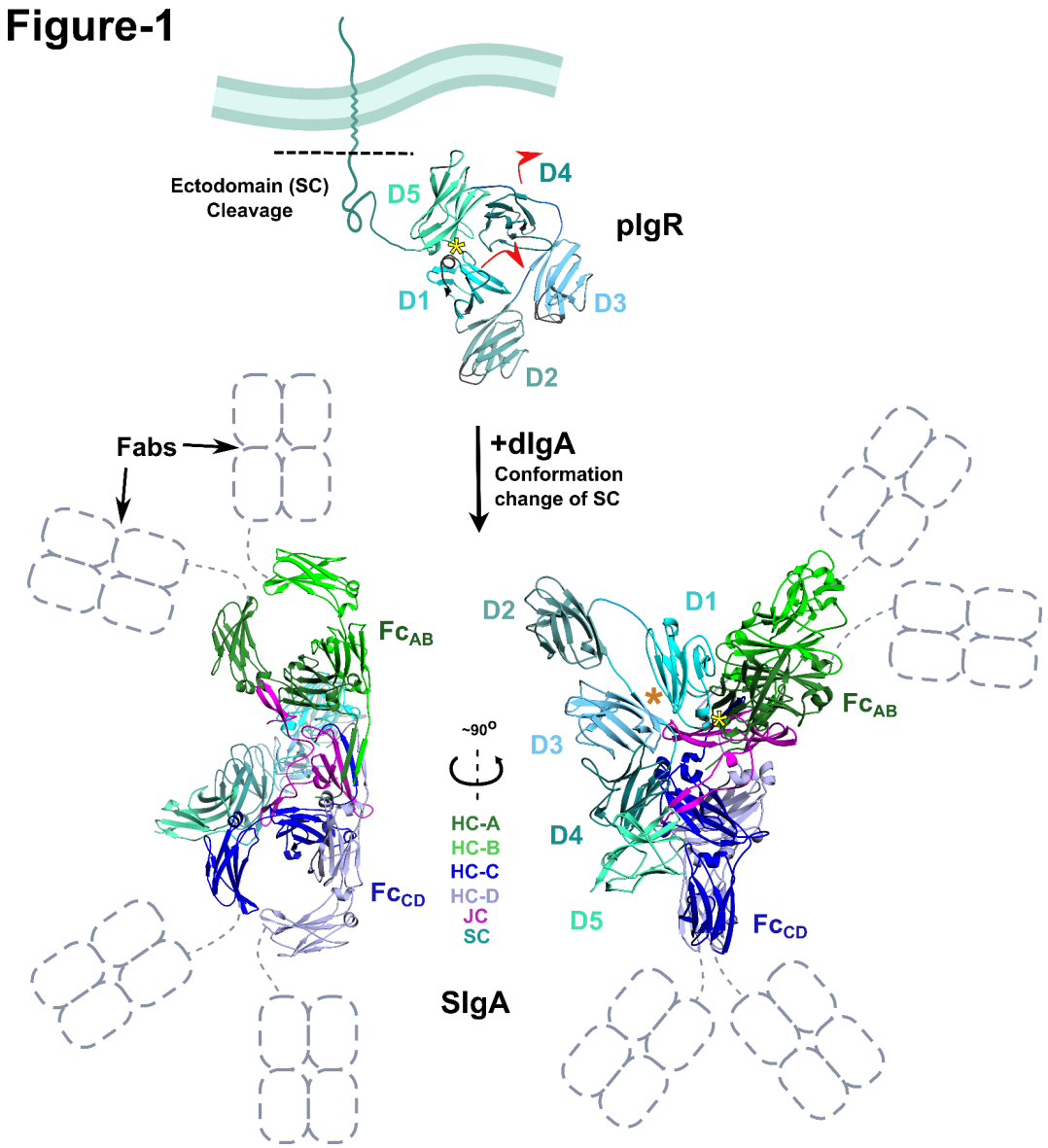

Figure-1: The structure of liganded and unliganded SC. (Top) Cartoon representation of a mouse pIgR ectodomain homology model based on the human SC crystal structure (PDB:5D4K). The pIgR is depicted bound to an epithelial cell membrane with its five constitutive immunoglobin-like domains (D1-D5) adopting a closed, unliganded conformation. Upon encountering dIgA, D1-D5 undergoes conformational change (indicated by red arrows) to form SIgA (PDB:7JG2), which is shown as a cartoon representation in two orientations (Fabs are disordered and represented with dotted schematics in grey). The dimeric SIgA contains four heavy chains (HC-A to D), J-chain (JC), and one Secretory Component (SC). All chains are colored according to the key. The Fc formed by HC-A and HC-B is indicated as Fc_{AB} (green) and the Fc formed by HC-C and HC-D is indicated as Fc_{CD} (of blue). The JC occupies the center of the SIgA complex with Fc_{AB} and Fc_{CD} on opposite sides of. The SC has five immunoglobin domains (D1-D5), and each domain (D1-D5) are colored with different shades of cyan. The yellow asterisk marks the location of D1 CDR loops in unliganded and liganded structures and the orange asterisk indicated the location of the D1-D3 interface in the liganded (SIgA) structure. Color scheme and labeling approach are adapted from S. Kumar Bharathkar *et al.*, "The structures of secretory and dimeric immunoglobulin A," *eLife*, vol. 9, p. e56098, Oct. 2020 [11].

53 Given critical roles in SIgA transport and function, the mechanisms of pIgR binding to pIgA have
54 long been of interest(8),(15),(16),(17),(18). Earlier studies demonstrated that pIgR (and SC) D1 is both
55 necessary and sufficient for binding to dIgA, but that D2-D5 further stabilize the SIgA
56 complex(15),(16),(18),(19), and structural and biophysical studies have demonstrated that pIgR/SC
57 domains undergo a massive conformational change upon dIgA binding (Fig.1) (8). The SIgA structures
58 further revealed contacts between D1 and Fc_{AB} (the Fcα formed by HC-A and HC-B) and TpC and TpD, as
59 well as D4-D5 contacts with Fc_{CD} (the Fcα formed by HC-C and HC-D)(11),(12),(13). Notably these
60 interactions were accompanied by new inter-domain contacts between D1-D3 and D3-D4 not observed in
61 the unliganded SC structure (Fig.S1). Furthermore, pIgR (and SC) binding to pIgA has long been
62 appreciated to require the JC(4),(20),(21). SIgA structures suggest that the JC directly provides contacts for
63 pIgR (or SC) D1 binding and indirectly provides the bent asymmetric conformation needed for other pIgR
64 (or SC) domains to bind(11),(12),(13).
65 Taken together, pIgR binding to pIgA can be described as a multi-step process involving multiple
66 interactions between pIgA and multiple SC domains (D1-D5), that undergo conformational changes to bind
67 four IgA HCs and the JC, while also forming new inter-domain contacts within SC (Fig.1, Fig.S1); yet,
68 aspects of this remarkably intricate mechanism remain unclear, such as the importance of inter-domain
69 contacts within SC (D1-D5), and the role of JC and Tps in pIgR/SC binding. Building upon recent structural
70 findings, we hypothesized that the conformational change-induced formation of pIgR/SC inter-domain
71 contacts, together with binding to the C terminus of JC is a critical step in SIgA assembly. To test this
72 hypothesis, we carried out structure-based mutational analysis combined with Surface Plasmon Resonance
73 (SPR) binding assays, that test the roles of pIgR/SC and JC residues in SIgA complex formation. Results
74 signify that formation of the D1-D3 interface and D1 binding to the C-terminal residues of JC and Tps are
75 pivotal steps necessary to achieve stable SIgA formation and subsequent effector functions.
76
77

RESULTS

To investigate the molecular mechanisms underlying SIgA assembly we analyzed existing SC(8), dIgA(11) and SIgA(11),(12),(13) structures and identified SC and JC residues with potential to mediate the pIgR binding mechanism, for example, residues that may promote SC conformational changes and/or stabilize SIgA interfaces. Subsequently, we mutated target residues in recombinantly expressed full-length SC and D1-only variants and tested binding to immobilized recombinant dIgA lacking the Fabs (dFcα) using SPR binding assays; we also tested unmutated SC and D1-only binding to dFcα containing JC mutant variants. SC and D1 analytes provide an established, soluble model for pIgR binding to dIgA(8). Consistent with the ligand-binding-induced conformational change observed for full-length SC, published SC-dIgA binding studies do not fit single state kinetic models, and thus similar to prior studies we followed the approach of qualitatively monitoring differences in the SPR binding profiles to identify differences among protein variants(8),(22), while also calculating equilibrium binding affinities for variants containing only D1. All experiments utilized mouse SC, Fcα and JC sequences.

D1-CDR3 plays a crucial role in the initiation of SC binding.

SC D1-D5 Ig-like domains each contain up to three loops (1-3) that are structurally similar to antibody complementarity determining regions (CDRs)(8). SIgA structures revealed residues in SC D1, including those in CDRs 1-3, mediating contacts with all four HCs and JC (Fig.S1C and Fig.S1F). However, the unliganded SC crystal structure revealed that a subset of these residues, including those in D1-CDR1 and CDR2, interact with D4 and D5 leaving them sterically occluded and likely unavailable to initiate binding between SC-D1 and dIgA, while D1-CDR3 is solvent exposed and does not participate in any interdomain interactions (Fig.S1C and Fig.S1F). This observation led us to hypothesize that D1-CDR3, which is solvent exposed and sterically accessible in unliganded SC, initiates pIgR binding to dIgA.

104

Figure-2

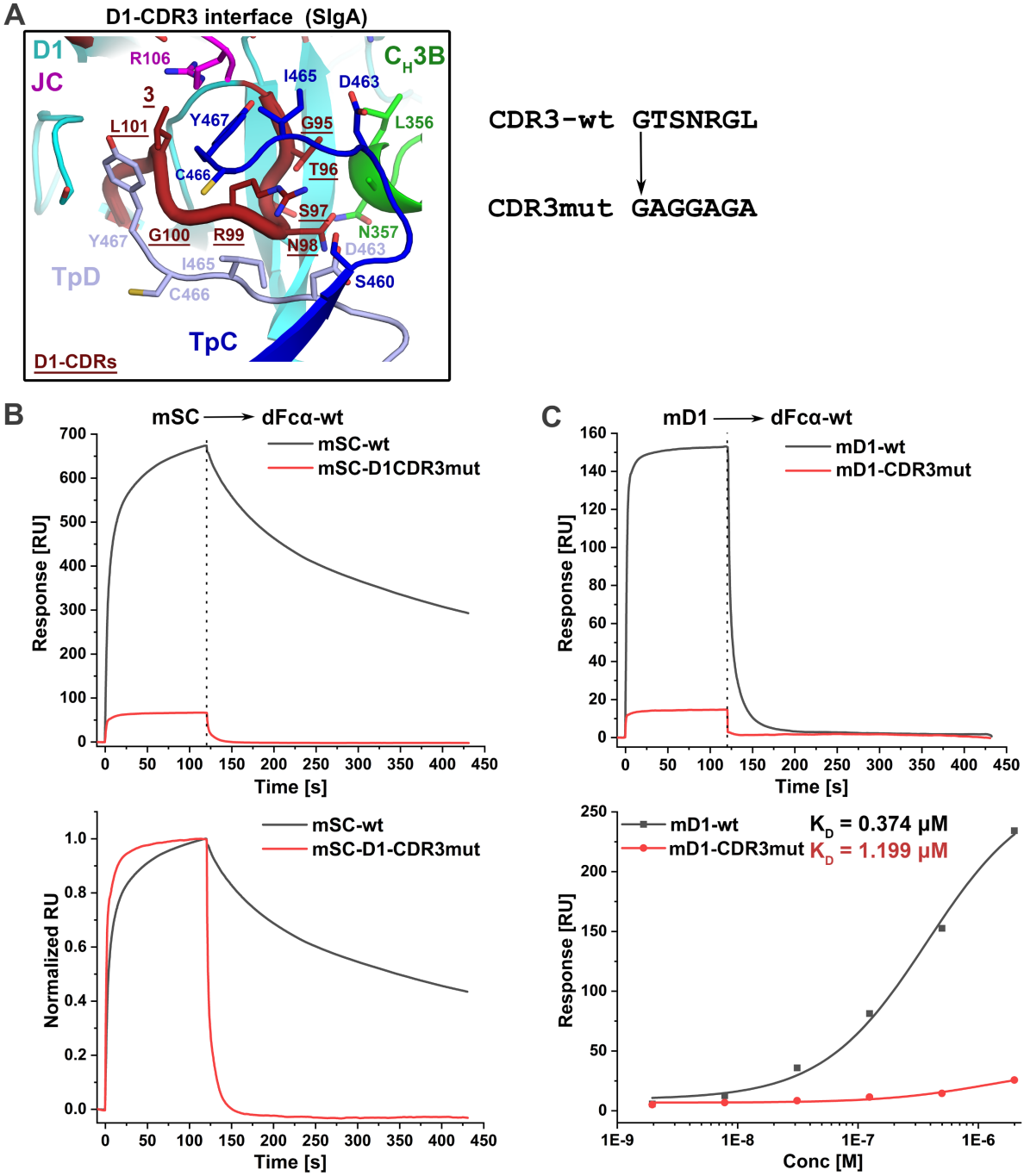

Figure-2: Contribution of mSC-D1-CDR3 towards binding dIgA. (A) Detailed view of mSC-D1-CDR3 and dIgA interactions found in mouse SIgA (PDB: 7JG2) (Fig.1, yellow asterisk); the structure is shown as a cartoon representation with interacting residues shown as sticks and labeled. D1-CDR3 residues that were mutated are underlined, and the unmutated and mutated sequences are shown on the right. (B) SPR sensorgrams showing the response (top) and normalized response (bottom) of 0.5uM mSC-wt (black) and mSC-D1-CDR3mut (red) binding to dFcα-wt. (C) SPR sensorgrams showing the response of 0.5uM of mD1-wt (black) and mD1-CDR3mut (red) binding to dFcα-wt (top) and the concentration dependent binding and steady state fit (bottom). The calculated K_D values for each analyte are indicated to the right of the name.

105 In SIgA structures, SC-D1-CDR3 residues contact HC-B, TpC and TpD though hydrogen bonds
106 and ionic interactions, and additionally, lie within 3.5-6Å of JC, where they may mediate Van-der Waals
107 interactions (Fig.2A). To explore the hypothesis that SC-D1-CDR3 is crucial for SC and dIgA binding, we
108 generated SC expression constructs, in which the SC-D1-CDR3 residues were mutated to Glycine and
109 Alanine (CDR3-wt: GTSNRGL to CDR3-mut: GAGGAGA), limiting the possible side chain interactions
110 with dIgA, while preserving the length of the loop (Fig.2A). The first construct incorporated this mutation
111 into full-length SC (mSC-D1-CDR3mut) and the second incorporated it into an expression construct
112 encoding only SC-D1 (mD1-CDR3mut). We expressed and purified variants along with unmutated controls,
113 mSC-wt and mD1-wt, and tested their binding to dFcα-wt (Fig.2 and Fig.S2).
114 The mSC-D1-CDR3mut SPR sensorgrams revealed markedly lower response units (RU) compared
115 to concentration-matched mSC-wt responses, with an overall maximal response (R_{max}) of mSC-D1-
116 CDR3mut that was 9.87% of the mSC-wt R_{max} for the 0.5μM analyte sample (Fig.2B and Fig.S2A).
117 Furthermore, overlay of normalized responses revealed more rapid association and dissociation for mSC-
118 D1-CDR3mut compared to mSC-wt (Fig.2B). Similarly, the mD1-CDR3mut SPR sensograms revealed
119 markedly lower response, ~9.6% of the concentration-matched mD1-wt response (Fig.2C, Fig.S2B) and an
120 overall reduction in affinity from K_D=0.374μM for mD1-wt to K_D=1.199μM for mD1-CDR3mut (Fig.2C).
121 In contrast to comparisons between mSC-D1-CDR3mut and concentration matched mSC-wt, the responses
122 revealed similar association and dissociation phases for mD1-CDR3mut and mD1-wt. Taken together, these
123 data indicate that mutations in D1-CDR3 reduce D1 binding affinity in the context of SC and isolated D1,
124 but alter the binding kinetics only in the context of SC. These results point toward a central role for D1-
125 CDR3 in promoting D1-dIgA interactions, but also a role in promoting changes in other SC domains upon
126 dIgA binding, as evidenced by differences in binding kinetics for mSC-wt and mSC-D1-CDR3mut. These
127 differences may result from conformational changes that expose more of D1 for binding and/or the binding
128 of other SC domains.
129
130

131 **The formation of the SC D1-D3 clamp is crucial for stabilization of SC-binding.**

132 In unliganded human SC, D1 forms extensive interfaces with SC domains D2, D4 and D5, yet
133 shares minimal contacts with D3 (no contacts in mouse SC, one contact in human SC)(8). However, in the
134 SIgA structure, D1 contacts only D3 through an extensive hydrophobic interface described as a "D1-D3
135 clamp" (Fig.3B)(11),(12),(13). The hydrophobic interface involves D1 residues F5, P7, Y23, P25 and D3
136 residues L226, Y228, F326. Notably, D3 L226 and Y228 contact SC D4 in the unliganded SC structure,
137 implying that D3 swaps interfaces between D4 (unliganded) and D1 (liganded) during SC binding in what
138 we hypothesize is a dominant step in SC's conformational change associated with SIgA formation (Fig.3A
139 and Fig.S1D, S1E).

140 To investigate the significance of the D1-D3 clamp, we generated three mutated SC variants to
141 minimize the hydrophobic interface: (1) mSC-D1mut, which includes D1 F5A, Y23A, and P25A mutations,
142 (2) mSC-D3mut, which includes D3 L226A, Y228A, F326A mutations, and (3) mSC-D1-D3mut, which
143 includes D1 F5A, Y23A, P25A and D3 L226A, Y228A, F326A mutations (Fig.3B) and tested their binding
144 to mouse dFcα-wt. Compared to mSC-wt, SPR sensorgrams revealed lower RUs and lower R_{max} for the
145 binding of concentration-matched mSC-D1mut (15.7% mSC-wt R_{max}), mSC-D3mut (25.3% mSC-wt R_{max}),
146 and mSC-D1-D3mut (20.7% mSC-wt R_{max}) (Fig.3C and Fig.S3), indicative of weaker binding.
147 Qualitatively, the reduction in RU appeared similar for all three mutant variants, with R_{max} values being
148 between 15-26% of mSC-wt for 0.5μM analytes; the combination of mutations in both D1 and D3 did not
149 appear to produce an additive effect, indicating that disruption of interface residues in either D1 or D3 was
150 sufficient to disrupt the interface.

151 Overlay of concentration matched, normalized responses for mSC-wt and mSC-mutant variants
152 also revealed differences in the binding kinetics, with mSC-D1mut exhibiting faster association and faster
153 dissociation phases compared to mSC-wt (Fig.3C). Responses of mSC-D1mut were similar to those of
154 mD1-wt (Fig.3C, Fig.3D), which may indicate that only D1 (and not D4 and D5) is binding. However,
155 mSC-D3mut and mSC-D1-D3mut exhibited association phases similar to mSC-wt, but faster dissociation
156 phases compared to mSC-wt. Compared to mSC-D1mut, mSC-D3mut and mSC-D1-D3mut exhibited

157 moderate differences in the dissociation phase compared to mSC-D1 mut, suggesting that mutation of the

158 D3 interface may impact binding differently than mutation of the D1 interface (Fig.3C and Fig.S3).

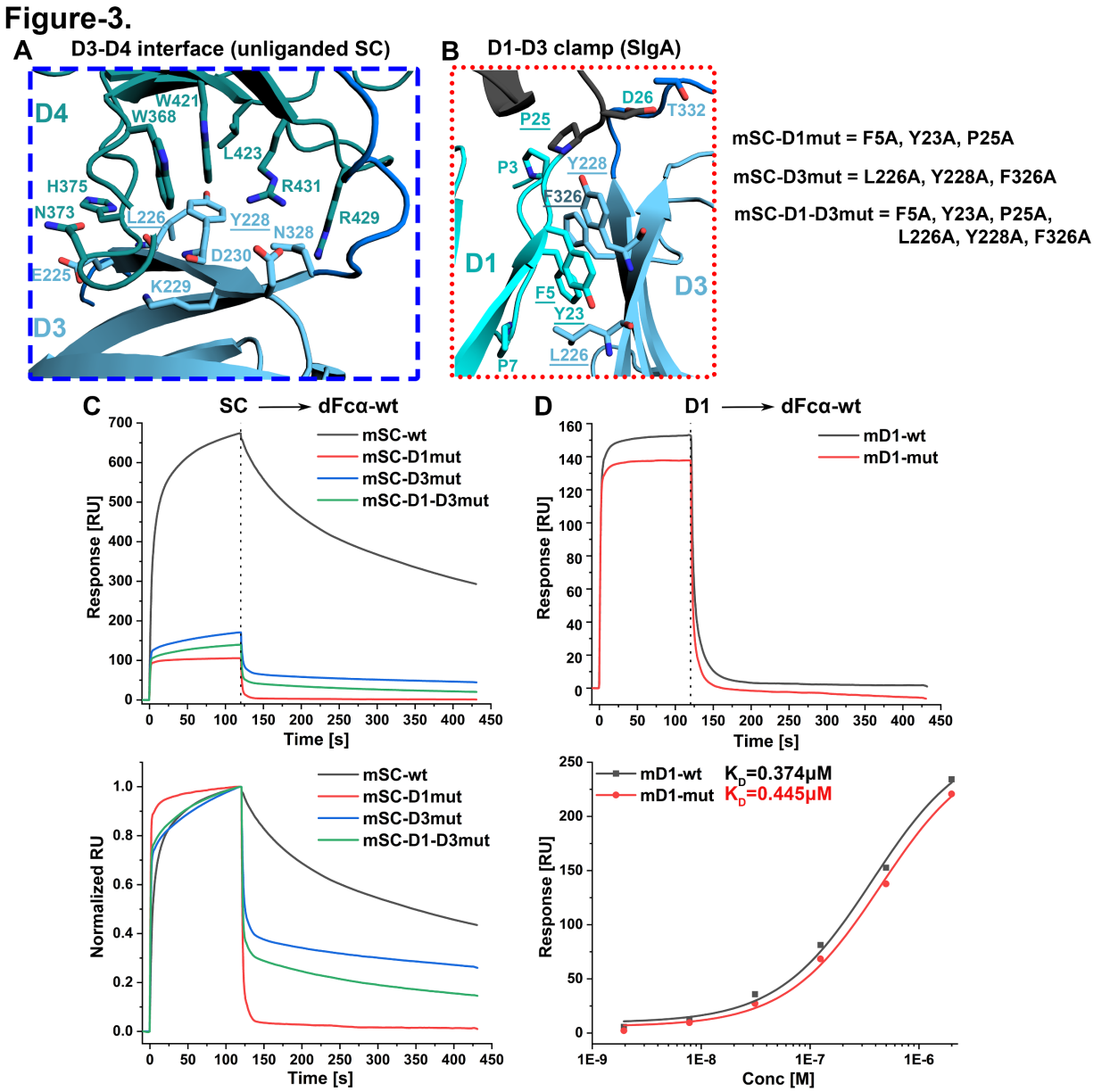

Figure-3: Role of SC-D1-D3 Clamp for the stabilization of SC and dIgA binding. (A) Detailed view of the unliganded D3-D4 interface from the homology model of mSC and the D1-D3 interface from the SIgA cryo-EM structure (Fig.1, orange asterisk) (PDB code 7JG2). In (A) and (B) structures are shown as a cartoon representation with interacting residues, shown as sticks and labeled. SC D1 and D3 residues that were mutated are underlined, and the unmutated and mutated sequences are shown on the right. (C) SPR sensorgrams showing the response (top) and normalized response (bottom) of 0.5uM mSC-wt (black) mSC-D1mut (red), mSC-D3mut (blue) and mSC-D1-D3mut (green) binding to dFcα-wt. (D) SPR sensorgrams showing the response of 0.5uM of mD1-wt (black) and mD1-mut binding to dFcα-wt (top) and the concentration dependent binding and steady state fit (bottom). The calculated K_D values for each analyte are indicated to the right of the name.

159 To explore the possibility that mutation of D1 F5A, Y23A, P25A influenced D1 binding
160 independent of the other SC domains we generated mD1-mut, which contained D1 F5A, Y23A and P25A
161 mutations, and compared its binding affinity to mD1-wt (Fig.3D and Fig.S3). The mD1-mut binding
162 affinity, K_D=0.445μM, was comparable to the mD1-wt binding affinity, K_D=0.374μM, indicating that D1
163 interactions with dIgA were not disrupted. Thus, in the context of full-length SC, the mutations F5A, Y23A
164 and P25A appear to reduce binding to dIgA indirectly, presumably through disruption of the D1-D3 clamp.
165 Taken together, results imply that D1-D3 interface formation contributes to stable SIgA assembly but is not
166 necessary for SC (or D1) binding. As noted, the kinetics of the three D1-D3 interface mutants closely
167 resemble that of isolated SC D1 (Fig.3 and Fig.S3) and thus it is plausible that disruption of the D1-D3
168 clamp prevents subsequent stages of SC binding (e.g., part of the conformation change and D4-D5 binding
169 to dIgA) resulting in only D1-dIgA contacts. Alternatively, D1-D3 clamp disruption may markedly decrease
170 the efficiency of SC D4-D5 binding and/or the stability of the resulting SIgA.
171
172 **JC C-terminal residues mediate pIgR binding to dIgA.**
173 The structures of human and mouse SIgA reveal similar conformations for SC, JC and similar
174 contacts between chains. Among these interactions, SC-D1 contacts with JC are conserved, and contribute
175 to 63% of the total SC- JC interface. Of the three SC-D1 CDRs, JC interfaces primarily with SC-D1-CDR1,
176 forming hydrogen bonds and ionic interactions between JC residues R106, D107, D132, Y135 and D137
177 and SC-D1-CDR1 residues S28, D30, R31, H32 and T33 (Fig.4A). JC Y135 and D137 are part of the
178 conserved C-terminal *YPD* motif that follows JC wing-2; JC-YPD are disordered in the dIgA structure(11)
179 and therefore we hypothesized that these residues play a dominant role in pIgR binding, rather than dIgA
180 assembly. Furthermore, in unliganded SC, D1-CDR1 R31 and H32 form contacts with D4-D5(Fig.S1C)(8)
181 and thus, JC YPD may function to displace the D1-D4D5 interface and/or promote D1-JC binding while
182 freeing D4-D5 to bind the Fc_{CD}. To investigate these possibilities, we created ten JC variants with mutations
183 or truncations in YPD.
184

Figure-4.

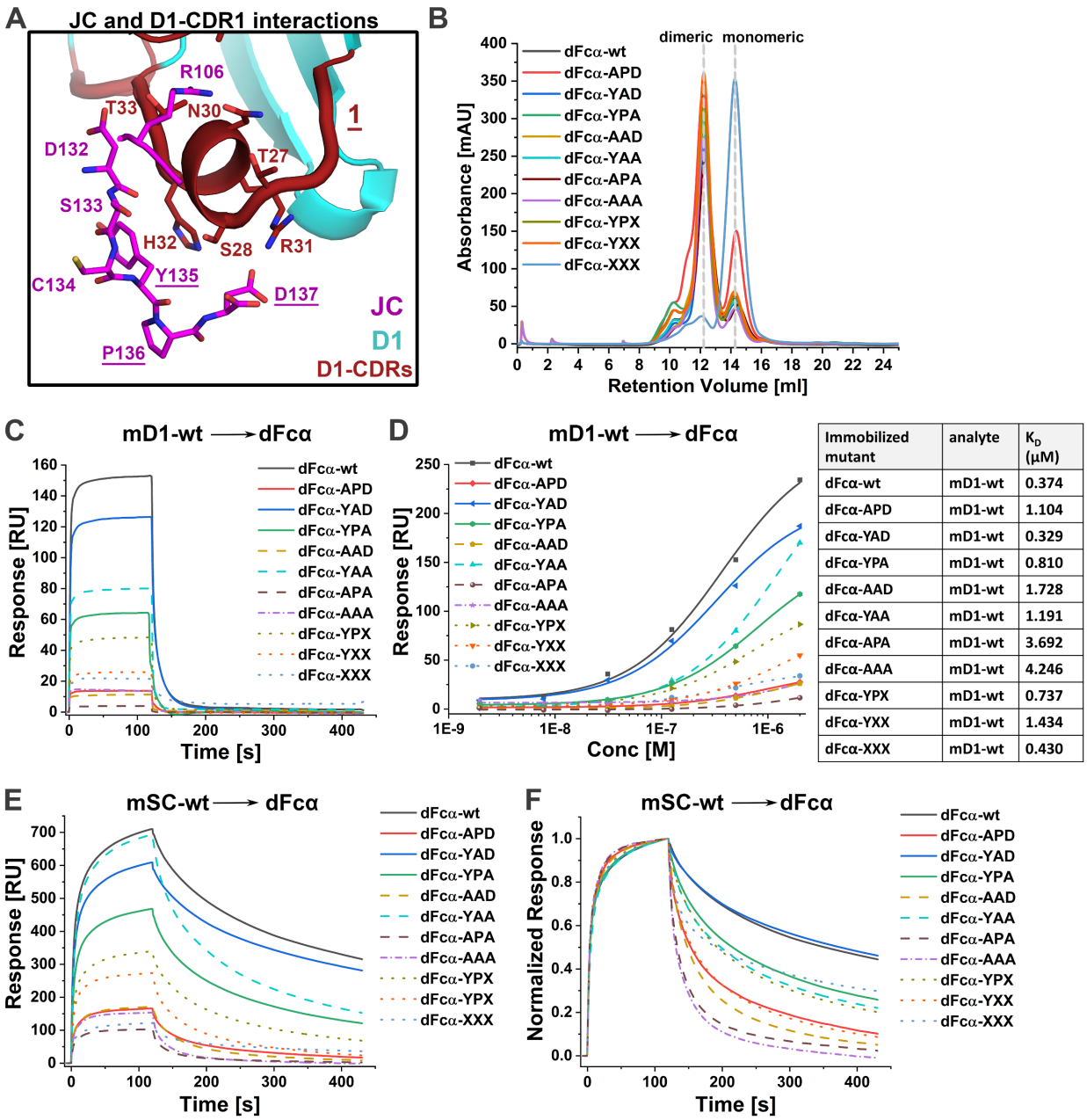

Immobilized mutant	analyte	K_D (μM)
dFcα-wt	mD1-wt	0.374
dFcα-APD	mD1-wt	1.104
dFcα-YAD	mD1-wt	0.329
dFcα-YPA	mD1-wt	0.810
dFcα-AAD	mD1-wt	1.728
dFcα-YAA	mD1-wt	1.191
dFcα-APA	mD1-wt	3.692
dFcα-AAA	mD1-wt	4.246
dFcα-YPX	mD1-wt	0.737
dFcα-YXX	mD1-wt	1.434
dFcα-XXX	mD1-wt	0.430

Figure-4: Role of the JC YPD motif in binding mSC-wt or mD1-wt. (A) The interaction of JC with SC-D1, and specifically D1-CDR1 shown as red loop with larger radius. The interacting residues are shown as sticks at this interface. Y135, P136 and D137 are underlined in JC, indicating that these residues were subjected to mutations, such as alanine substitutions or truncations. (B) The SEC chromatograms of the indicated dFcα-wt and dFcα mutant variants resulting from 25ml co-transfections and following Nickel-NTA purification; fractions corresponding to dimeric forms were used for SPR experiments. (C) SPR sensorgrams of 0.5uM mD1-wt binding to the indicated dFcαs with JC- YPD alanine mutations or truncations. (D) The steady state affinity analysis of mD1-wt binding to the indicated wt or mutant dFcα variants. The respective calculated K_D values are listed in the adjacent table. (E) SPR sensorgrams of 0.5uM mSC-wt binding to different dFcα with JC- YPD alanine mutations or truncations. (F) SPR sensorgrams showing the normalized response of 0.5uM mSC-wt analytes binding to the indicated dFcα variants.

185

186 Initially we tested the effect of YPD mutations or truncations on dFcα assembly by co-expressing
187 each JC variant with Fcα and found that all could be incorporated into dFcα, indicating that mutations did
188 not inhibit dFcα assembly. In most cases, the relative percentage of dFcα and monomeric Fcα, which is
189 found in lower abundance in all dFcα preparations, was similar for preparations containing unmutated or
190 mutated JC. However, truncation of YPD resulted in higher percentages of monomeric Fcα and lower dFcα
191 yield, suggesting that the efficiency of JC incorporation, and therefore dIgA assembly, may rely in-part on
192 the presence of JC C-terminal residues (Fig.4B). Accordingly, we used mutated dFcα variants as
193 immobilized ligands in mD1-wt and mSC-wt SPR binding assays.

194 Initially, we tested binding of mD1-wt to dFcα-wt and dFcα-mutant variants having single (dFcα-
195 APD, dFcα-YAD, dFcα-YPA), double (dFcα-AAD, dFcα-ADA, dFcα-YAA) or triple (dFcα-AAA) alanine
196 substitutions in JC YPD and calculated the binding affinity for each variant. Results revealed binding
197 affinities of K_D=0.374μM, K_D = 1.104uM, K_D = 0.329uM and K_D = 0.810uM for dFcα-wt and single alanine
198 variants dFcα-APD, dFcα-YAD, and dFcα-YPA, respectively (Fig.4C, Fig.4D). Binding affinities for
199 double mutants dFcα-AAD, dFcα-APA, and dFcα-YAA were K_D =1.728uM, K_D =3.692uM and K_D =1.191
200 uM, respectively (Fig.4C, Fig.4D). Collectively, these results demonstrate a marked reduction in binding
201 affinity when either Y135 or D137 is mutated and a further reduction in binding affinity when both Y135
202 and D137 are mutated to alanine. The P136A mutation resulted in a comparatively minor changes in binding
203 on its own; however, did further reduce binding when combined with Y135A or D137A mutations. The
204 binding affinity for the triple mutant dFcα-AAA was K_D = 4.246uM, indicating the substitution of all YPD
205 residues has the most pronounced effect on binding (Fig.4C, Fig.4D).

206 We also tested the mSC-wt binding to all dFcα YPD-alanine substitutions. Although resulting SPR
207 responses do not fit a single-state kinetic model or reach equilibrium during the experiment, differences in
208 dissociation phases for concentration matched, normalized responses were apparent when comparing mSC-
209 wt binding to dFcα-wt and dFcα YPD-alanine substitutions (Fig.4E, Fig.4F). Specifically, we observed that
210 all mutations except P136A altered dissociation. Consistent with experiments that tested D1 binding, single
211 mutation Y135A exhibited the most pronounced effect, followed closely by D137A; the combination of

212 Y135A and D137A further altered the dissociation phase (more rapid dissociation) and the triple mutant
213 containing Y135A, P136A, and D137A exhibited the most significant change in dissociation compared to
214 unmutated control, dFcα-wt. Qualitatively, we also observed subtle differences in association and overall
215 reduction in R_{max} values for mSC-wt binding to the majority of dFcα YPD-alanine substitutions (Fig.4E and
216 Fig.S4).

217 Taken together YPD-alanine substitutions reveal a central role for JC-YPD in mediating D1 binding
218 to dIgA. Y135 and D137 appear to play prominent and unique roles since individual mutations in these
219 residues reduced binding affinity more than mutation of P136. Both Y135 and D137 appear to contribute
220 uniquely since dFcα YPD-alanine substitutions that combined them exhibited further reductions in binding.
221 While a more minor role for P136 was observed, its mutation to alanine did reduce binding affinity, most
222 notably when combined with the Y135A and/or D137A mutations. Notably, none of the dFcα YPD-alanine
223 substitutions completely abrogated mD1-Wt or mSC-wt binding indicating that either YPD main-chain
224 interactions and/ or other JC-SC interfaces are sufficient for SIgA formation.

225 To investigate the role of JC length and YPD main chain atoms on interactions with SC, we tested
226 SC binding to JC deletion mutants, in which D137 (dFcα-YPX), P136 and D137 (dFcα-YXX), or Y135,
227 P136 and D137(dFcα-XXX) were deleted. Initially, we tested mD1-wt binding to dFcα-wt and dFcα YPD
228 deletions, dFcα-YPX, dFcα-YXX and dFcα-XXX and calculated associated binding affinities. Results
229 revealed binding affinities of K_D= 0.737uM, K_D= 1.434uM and K_D= 0.430uM for dFcα-YPX, dFcα-YXX
230 and dFcα-XXX, respectively (Fig.4C, Fig.4D), indicating a reduction in binding upon the deletion of one
231 or more JC C-terminal residues compared to dFcα-wt K_D=0.374μM. Reduction in binding affinity was not
232 correlated with the number of deleted residues indicating that a change in length has some unknown impact
233 on D1 binding. We also tested the mSC-wt binding to all dFcα YPD-deletion variants and similar to dFcα
234 YPD alanine substitutions, observed differences in the dissociation phases for concentration matched,
235 normalized responses when comparing mSC-wt binding to dFcα-wt, dFcα-YPX, dFcα-YXX and dFcα-
236 XXX (Fig.4E, Fig.4F). While we observed more rapid dissociation for mSC-wt binding to dFcα-YPX and
237 dFcα-YXX (compared to dFcα-wt), binding to dFcα-XXX exhibited dissociation more similar to dFcα-wt,

238 albeit still altered. Taken together, these results further support a role for JC YPD in SIgA formation and
239 suggest that both sidechain identity and the presence of mainchain atoms support the interaction.
240

241 **DISCUSSION**

242 The pIgR binding to dIgA is a critical step in SIgA formation, its transcytosis to mucosal secretions,
243 and downstream effector functions(23),(24). Prior work has unveiled an intricate, multi-step process, in
244 which domains D1-D5 undergo conformational rearrangements that uncover D1 residues, ultimately
245 allowing them to bind all four HCs and the JC, while also repositioning D4 and D5 to bind a single HC(8),
246 (11),(12),(13),(16),(17),(18). Here we characterized the contributions of specific residues in the D1 CDR3,
247 the D1-D3 clamp and the JC C-terminal YPD residues, which provide new details on how SIgA assembles.

248 In SIgA, D1-CDR3 residues account for just 34.3% of D1's total buried surface, yet in our studies
249 mutation of these residues reduced D1 binding affinity by ~3 times and altered SC association and
250 dissociation phases. Prior studies demonstrated that D1 is necessary and sufficient for dIgA
251 binding(16),(19), and that substituting the highly conserved D1 CDR loops with alternative sequences (e.g.
252 from other SC domains) resulted in limited dIgA binding (18). D1 CDR1, which contains a conserved
253 helical turn has long been thought to play a pivotal role in the process(15),(18); however, our data and
254 analysis also point toward a central role for D1-CDR3 in SIgA assembly. As noted, D1-CDR3 residues,
255 unlike D1-CDR1 and D1-CDR2 residues, are fully exposed in the unliganded SC structure(8) and thus, our
256 results are consistent with the model in which exposed D1-CDR3 residues are able to initiate binding by
257 contacting Tps and JC residues, promoting D1-CDR1 and D1-CDR2 contact with dIgA, and likely initiating
258 the conformational change. CDR3 residues also appear to contribute considerable stability to SC
259 interactions with pIgA in the fully assembled structure and interface with at least four different chains. In
260 the mouse SIgA structure(11), SC-D1-CDR3 residues participate in a network of hydrogen bonds and ionic
261 interactions with HC-B, TpC, and TpD as well as putative Van-der Waals interactions with the JC.
262 Furthermore, these Tps (specifically TpD) and JC residues appear to be flexible (disordered) in dIgA and

263 we speculate that binding to CDR3 helps stabilize their positions and following the conformational change
264 and promote additional interactions with D1 (e.g. CDR1 and CDR2).

265 D1-CDR3 may also promote binding to higher order pIgA and pIgM. Our own inspection of the
266 human dimeric (PDB: 6UE7 and 6LX3)(12),(13), tetrameric (PDB: 6UE8 and 6UE9), and pentameric
267 (PDB:6UEA) SIgA core structures(12), reveals D1-CDR3 contacting one Tp (the others are not resolved)
268 in dimeric SIgA and contacting two Tps in tetrameric and pentameric SIgA; in pentameric SIgA, a third Tp
269 contacts D1 outside the CDR regions (11),(12),(13). These observations are consistent with earlier reports
270 that SC bound tetrameric IgA2m2 with better affinity than dimeric IgA1 and dimeric IgA2m1(5) and
271 suggest D1-CDR3 may support high affinity binding to higher order pIgA. Our inspection of the related
272 SIgM core structure (PDB: 6KXS and 7K0C)(25),(26) indicates that SC D1 forms additional contacts with
273 the Tps in pentameric SIgM (similar to pentameric SIgA and in contrast to dimeric SIgA) and thus evolution
274 of D1 may have been driven by interactions with higher order polymers of IgM and IgA and their respective
275 Tps.

276 The structures of SIgA (and SIgM) revealed that the pIgR's ligand-induced conformational change
277 is associated with the formation of the D1-D3 clamp and data presented here revealed that disruption of the
278 D1-D3 clamp markedly reduces dIgA binding. Structurally, the unliganded SC D3-D4 interface must be
279 disrupted for D1-D3 interface to form, which implies that either the D1-D3 interface formation frees D4-
280 D5 for binding to dIgA, or that the binding of D4-D5 to dIgA frees D3 to bind D1. Indeed, SC variants with
281 mutated clamp residues exhibited SPR binding profiles that are similarly to that of D1 only, which may
282 indicate that in the absence of the clamp, D4 and D5 are not able to bind efficiently. While this could result
283 from failure of the clamp to form and/or from the failure of the unliganded SC D3-D4 interface to break; it
284 is notable that among D1-D3 interface mutants, mSC-D1mut is the weakest binder. The mSC-D1mut lacks
285 the L226A and Y228A mutations found in mSC-D3mut and mSC-D1-D3mut, which are expected to disrupt
286 the D3-D4 interface in unliganded SC. Thus, it appears plausible that D1-D3 clamp formation frees D4 and
287 D5 and positions them optimally to bind dIgA. Regardless, it is clear is that both disruption of unliganded

288 SC D3-D4 contacts and formation of the liganded D1-D3 clamp and are crucial for the formation of a stable
289 SIgA complex.

290 The JC has long been known to be necessary for dIgA assembly in mammals and for pIgR binding
291 to dIgA; yet gaps in our understanding of how it mediates both processes remain (27). The mouse dIgA
292 structure revealed numerous contacts between JC and two copies of mIgA; however, the conserved C-
293 terminal JC YPD motif was disordered (11), hinting at a limited role in dIgA assembly. Our data
294 demonstrate that dIgA assembly can tolerate mutations in JC YPD, and thus, its identity is not necessary
295 for dIgA assembly. A limited role for the JC C-terminus in dIgA is consistent with earlier studies, in which
296 deletion of the 25 or more residues from the C-terminus did not completely abrogate polymeric IgA
297 assembly (21). However, our data indicates the presence of three C-terminal residues in the YPD location
298 may contribute significantly to the dIgA assembly process since deletion of all three residues resulted in
299 markedly lower levels of dIgA expression. Additionally, the mouse SIgA structure revealed an ordered YPD
300 motif contacting SC-D1 (11) and we find that mutations of these residues, particularly Y and D, markedly
301 impact SC binding. Yet, mutation or deletion of JC YPD doesn't completely inhibit SC binding *in vitro*.
302 Thus, other contacts between the JC and SC and/or dIgA appear to be sufficient for binding in our
303 experiments. While these contacts may include other JC-SC interfaces, it may also be that SC-SC and/or
304 SC-HC contacts help compensate for JC mutations and that those contacts are dependent on the overall bent
305 dIgA conformation, conferred by largely by the JC (but not directly by the YPD). Regardless, our data
306 support the notion that direct contacts with the JC C-terminal YPD motif are an inherent part of the pIgR-
307 dIgA binding mechanism.

308 Notably, none of our SC or JC mutant variants completely abrogated SC-dIgA binding. This is
309 valuable for determining the relatively contributions of mutated residues; however, we also speculate that
310 the reductions in binding affinity and apparent changes in kinetics that we observe could translate to severe
311 disruption of pIgR-dependent transcytosis and or reduced SIgA stability in the mucosa. For example,
312 mutations in the D1-D3 clamps and/or mutations disrupting interfaces may increase the exposure and/or
313 flexibility of SC and/or dIgA motifs making them more susceptible to proteolysis. They may also limit

314 subsequent stages of pIgR binding to dIgA. For example, mD5 C470 (C468 in human) can form a disulfide
315 bond with HC C306 (C311 in human IgA) that stabilizes SIgA after SC D5 has bound dIgA
316 (11),(12),(13),(28),(29). As noted in our results, mutations in SC D1 and/or D3 resulted in kinetic profiles
317 similar to D1 only variants, and thus we speculate that these mutations may limit D4/D5 binding and
318 subsequent disulfide bond formation; however, in our SPR experiments (and previously reported binding
319 studies (8),(22)) SC C470 and C504 were mutated to alanine to prevent irreversible binding to dIgA
320 surfaces.
321

322 **MATERIALS AND METHODS**

323 **Construct design and cloning**

324 To make the mouse Fcα expression construct, the gene segment encoding the *mus musculus* IgA
325 HC constant region (Uniprot P01878) CH2 and CH3 domains was codon optimized, fused to an N-terminal
326 TPA signal sequence (residues MDAMKRGLCCVLLLCGAVFVSPAGA) and a C-terminal hexahistidine
327 affinity tag and cloned into expression vector pD2610v1 (ATUM) using Electra cloning (ATUM),
328 analogous to previously reported full-length IgA HC expression constructs(11). Constructs encoding the
329 *mus musculus* JC (Uniprot P01592; native signal peptide) and *mus musculus* pIgR ectodomain residues 1-
330 567 (Uniprot P01592; native signal peptide), were used as previously reported and served as templates for
331 cloning truncated and/or mutant variants(11). SC and JC mutations were introduced into coding sequence
332 fragments using overlap-extension PCR(30) with primers encoding the desired mutations (Integrated DNA
333 Technologies; IDT) and Electra cloning sites; resulting products were cloned into expression vector
334 pD2610v1 (ATUM) using Electra cloning (ATUM). SC-D5 cysteine mutations (C470A and C504A) were
335 introduced into all SC expression constructs to prevent the formation of disulfide bonds with dIgA, as
336 previously described(8). Constructs encoding the SC mD1-wt (residues 1-117) and mD1-mutant variants
337 were generated by PCR and overlap extension PCR as described for other SC variants; coding sequence
338 retained the native signal peptide and a C-terminal hexahistidine tag and were cloned into pD2610v1 using
339 Electra cloning (ATUM).

340 **Protein expression and purification**

341 All constructs were transiently transfected (SC and D1 variants) or co-transfected (Fcα and JC) into
342 Expi293F (Gibco: A14527) cells using the ExpiFectamine 293 Transfection kit (Gibco: A14525) and
343 following previously described methods (11). Four to five days after transfection, supernatants were
344 harvested and filtered through 0.22µm PES bottletop filters (Millipore Sigma). Proteins and complexes
345 were purified from the cell supernatants using Nickel-NTA affinity resin (Qiagen: 30210), followed by
346 Superose 6 (Cytiva) or Superdex 200 (Cytiva) size exclusion chromatography (SEC) on an AKTA FPLC
347 (Cytiva). During and after SEC, purified molecules were maintained in TRIS-buffered saline (20mM Tris+
348 150mM NaCl, pH=7.4). The SEC-eluted protein peaks corresponding to the correct retention volume based
349 on the molecular weight standards (BioRad: 1511901) were collected, concentrated using Amicon Ultra
350 centrifugal filters (Millipore Sigma) to stock concentrations between 2-4mg/ml for SC, 1.5-2mg/ml for D1,
351 and 0.4-0.7mg/ml for dFcα constructs, which were then filtered using 0.22µm spin filters (Millipore Sigma)
352 and utilized for SPR experiments.

353

354 **SPR experiments and data analysis.**

355 SPR experiments were carried out using a Sierra SPR-32 Pro (Bruker) operating at room
356 temperature. Solutions containing 0.25uM dFcα-wt or dFcα mutant variant ligands in sodium acetate buffer
357 (pH=4), were immobilized on lanes B1-8 and D1-8 of a High-Capacity Amine (HCA) 32-spot sensor
358 (Bruker) using a standard amine coupling kit (Bruker). Lanes A and C were mock coupled using sodium
359 acetate buffer pH=4 and served as references. The binding of soluble analytes, including mSC-wt, mSC-
360 mutants, mD1-wt and mD1-mutants was tested using a two-fold (mSC and variants) or four-fold (mD1 and
361 variants) dilution series starting at 2uM in HBS-EP+ running buffer (0.01 M HEPES, 0.15 M NaCl, 3 mM
362 EDTA, 0.005% v/v Surfactant P20, pH 7.4). Analyte responses were measured on all spots and responses
363 on lanes A and C (internal references) were subtracted to account for any non-specific binding. Kinetic
364 experiments were carried out using a 25ul/min flow rate, 120s contact time, and 300s dissociation time.

365 After every cycle the surface was regenerated using 2.5M MgCl2 three times, followed by a wash step with
366 the running buffer (HBS-EP+) to achieve the best baseline for the next cycle.

367 Resulting SPR data were analyzed using the Bruker Sierra Analyzer software version R4. Briefly,
368 all data were reference subtracted and buffer-subtracted and K_D values were calculated for the D1-only
369 constructs using "steady state affinity" analysis program and 1:1 Langmuir + offset fitting model. Raw
370 sensor-grams (Response Units versus time) for all data and the steady state affinity data for mD1 variants
371 (Response Units vs concentration), were exported and re-plotted using OriginPro 2020 graphing and
372 analysis software (OriginLab: https://www.originlab.com/). Normalization of the respective sensorgrams
373 for concentration matched samples were carried out in OriginPro 2020, by dividing RU by R_{max} of the
374 respective analyte. Figures were assembled and in Photoshop (Adobe) or Inkscape (https://inkscape.org/).

375

376 **AUTHOR CONTRIBUTIONS**

377 The study was conceived by B.M.S and S.K.B.; experiments were conducted by S.K.B; Authors contributed
378 to data analysis and manuscript writing.

379

380 **ACKNOWLEDGEMENTS**

381 We thank Paul Ritter and Hniang Khamh for help with SPR training and troubleshooting, Sarah Leonard
382 for technical assistance, and members of the Stadtmueller Lab for insightful discussions regarding this
383 work. This work was supported by NIH grant R01AI165570 to B.M.S., University of Illinois start-up
384 funding to B.M.S., and the Lowell P. Hager Fellowship to S.K.B.

385 **REFERENCES**

386 1. Corthesy, B. 2013. Multi-Faceted Functions of Secretory IgA at Mucosal Surfaces. *Frontiers in*
387 *Immunology* 4.
388 2. Mantis, N. J., N. Rol, and B. Corthésy. 2011. Secretory IgA's complex roles in immunity and mucosal
389 homeostasis in the gut. *Mucosal Immunol* 4: 603–611.
390 3. de Sousa-Pereira, P., and J. M. Woof. 2019. IgA: Structure, Function, and Developability. *Antibodies* 8:
391 57.
392 4. Zikan, J., J. Mestecky, R. Kulhavy, and J. C. Bennett. 1986. The stoichiometry of J chain in human
393 secretory dimeric IgA. *Molecular Immunology* 23: 541–544.
394 5. Lombana, T. N., S. Rajan, J. A. Zorn, D. Mandikian, E. C. Chen, A. Estevez, V. Yip, D. D. Bravo, W.
395 Phung, F. Farahi, S. Viajar, S. Lee, A. Gill, W. Sandoval, J. Wang, C. Ciferri, C. A. Boswell, M. L.
396 Matsumoto, and C. Spiess. 2019. Production, characterization, and in vivo half-life extension of
397 polymeric IgA molecules in mice. *mAbs* 11: 1122–1138.
398 6. Kaetzel, C. S., J. K. Robinson, K. R. Chintalacharuvu, J. P. Vaerman, and M. E. Lamm. 1991. The
399 polymeric immunoglobulin receptor (secretory component) mediates transport of immune complexes
400 across epithelial cells: a local defense function for IgA. *Proc Natl Acad Sci U S A* 88: 8796–8800.
401 7. Brandtzaeg, P. 2013. Secretory IgA: Designed for Anti-Microbial Defense. *Frontiers in Immunology* 4.
402 8. Stadtmueller, B. M., K. E. Huey-Tubman, C. J. López, Z. Yang, W. L. Hubbell, and P. J. Bjorkman.
403 2016. The structure and dynamics of secretory component and its interactions with polymeric
404 immunoglobulins. *eLife* 5: e10640.
405 9. Asano, M., N. Takenouchi-Ohkubo, N. Matsumoto, Y. Ogura, H. Nomura, H. Suguro, and I. Moro.
406 2004. Multiple cleavage sites for polymeric immunoglobulin receptor. *Immunology* 112: 583–589.
407 10. Woof, J. M., and M. W. Russell. 2011. Structure and function relationships in IgA. *Mucosal Immunol*
408 4: 590–597.
409 11. Kumar Bharathkar, S., B. W. Parker, A. G. Malyutin, N. Haloi, K. E. Huey-Tubman, E. Tajkhorshid,
410 and B. M. Stadtmueller. 2020. The structures of secretory and dimeric immunoglobulin A. *eLife* 9:
411 e56098.
412 12. Kumar, N., C. P. Arthur, C. Ciferri, and M. L. Matsumoto. 2020. Structure of the secretory
413 immunoglobulin A core. *Science* 367: 1008–1014.
414 13. Wang, Y., G. Wang, Y. Li, Q. Zhu, H. Shen, N. Gao, and J. Xiao. 2020. Structural insights into
415 secretory immunoglobulin A and its interaction with a pneumococcal adhesin. *Cell Res* 30: 602–609.
416 14. Brunke, C., S. Lohse, S. Derer, M. Peipp, P. Boross, C. Kellner, T. Beyer, M. Dechant, L. Royle, L. P.
417 Liew, J. H. Leusen, and T. Valerius. 2013. Effect of a tail piece cysteine deletion on biochemical and
418 functional properties of an epidermal growth factor receptor-directed IgA2 m(1) antibody. *mAbs* 5: 936–
419 945.
420 15. Hamburger, A. E., A. P. West, and P. J. Bjorkman. 2004. Crystal Structure of a Polymeric
421 Immunoglobulin Binding Fragment of the Human Polymeric Immunoglobulin Receptor. *Structure* 12:
422 1925–1935.
423 16. Frutiger, S., G. J. Hughes, W. C. Hanly, M. Kingzette, and J. C. Jaton. 1986. The amino-terminal
424 domain of rabbit secretory component is responsible for noncovalent binding to immunoglobulin A
425 dimers. *Journal of Biological Chemistry* 261: 16673–16681.
426 17. Braathen, R., V. S. Hohman, P. Brandtzaeg, and F.-E. Johansen. 2007. Secretory Antibody Formation:
427 Conserved Binding Interactions between J Chain and Polymeric Ig Receptor from Humans and
428 Amphibians1. *The Journal of Immunology* 178: 1589–1597.
429 18. Coyne, R. S., M. Siebrecht, M. C. Peitsch, and J. E. Casanova. 1994. Mutational analysis of polymeric
430 immunoglobulin receptor/ligand interactions. Evidence for the involvement of multiple complementarity
431 determining region (CDR)-like loops in receptor domain I. *Journal of Biological Chemistry* 269: 31620–
432 31625.

19. Norderhaug, I. N., F.-E. Johansen, P. Krajči, and P. Brandtzaeg. 1999. Domain deletions in the human polymeric Ig receptor disclose differences between its dimeric IgA and pentameric IgM interaction. *European Journal of Immunology* 29: 3401–3409.
20. Vaerman, J.-P., A. E. Langendries, D. A. Giffroy, C. S. Kaetzel, C. M. Tamer Fiani, I. Moro, P. Brandtzaeg, and K. Kobayashi. 1998. Antibody against the human J chain inhibits polymeric Ig receptor-mediated biliary and epithelial transport of human polymeric IgA. *European Journal of Immunology* 28: 171–182.
21. Johansen, F.-E., R. Braathen, and P. Brandtzaeg. 2001. The J Chain Is Essential for Polymeric Ig Receptor-Mediated Epithelial Transport of IgA1. *The Journal of Immunology* 167: 5185–5192.
22. Stadtmueller, B. M., Z. Yang, K. E. Huey-Tubman, H. Roberts-Mataric, W. L. Hubbell, and P. J. Bjorkman. 2016. Biophysical and biochemical characterization of avian secretory component provides structural insights into the evolution of the polymeric Ig receptor. *J Immunol* 197: 1408–1414.
23. Johansen, F.-E., and C. S. Kaetzel. 2011. Regulation of the polymeric immunoglobulin receptor and IgA transport: new advances in environmental factors that stimulate pIgR expression and its role in mucosal immunity. *Mucosal Immunology* 4: 598–602.
24. Wei, H., and J.-Y. Wang. 2021. Role of Polymeric Immunoglobulin Receptor in IgA and IgM Transcytosis. *Int J Mol Sci* 22: 2284.
25. Kumar, N., C. P. Arthur, C. Ciferri, and M. L. Matsumoto. 2021. Structure of the human secretory immunoglobulin M core. *Structure* 29: 564-571.e3.
26. Li, Y., G. Wang, N. Li, Y. Wang, Q. Zhu, H. Chu, W. Wu, Y. Tan, F. Yu, X.-D. Su, N. Gao, and J. Xiao. 2020. Structural insights into immunoglobulin M. *Science* 367: 1014–1017.
27. Hockenberry, A., E. Slack, and B. M. Stadtmueller. 2023. License to Clump: Secretory IgA Structure–Function Relationships Across Scales. *Annual Review of Microbiology* 77: 645–668.
28. Chintalacharuvu, K. R., A. S. Tavill, L. N. Louis, J. P. Vaerman, M. E. Lamm, and C. S. Kaetzel. 1994. Disulfide bond formation between dimeric immunoglobulin A and the polymeric immunoglobulin receptor during hepatic transcytosis. *Hepatology* 19: 162–173.
29. Underdown, B. J., J. De Rose, and A. Plaut. 1977. Disulfide bonding of secretory component to a single monomer subunit in human secretory IgA. *J Immunol* 118: 1816–1821.
30. Ho, S. N., H. D. Hunt, R. M. Horton, J. K. Pullen, and L. R. Pease. 1989. Site-directed mutagenesis by overlap extension using the polymerase chain reaction. *Gene* 77: 51–59.

464 **Supplementary Information for:**

465 **Structural and biochemical requirements for secretory component interactions with**

466 **dimeric Immunoglobulin A**

467 Sonya Kumar Bharathkar and Beth M. Stadtmueller[1,2,3*]

468 [1]Department of Biochemistry, University of Illinois Urbana-Champaign, Urbana, Illinois 61801 USA

469 [2]Department of Biomedical and Translational Sciences, Carle Illinois College of Medicine, University of

470 Illinois Urbana-Champaign, Urbana, Illinois 61801 USA

471 [3]Carle R. Woese Institute of Genomic Biology

472 *Address correspondence to bethms@illinois.edu–

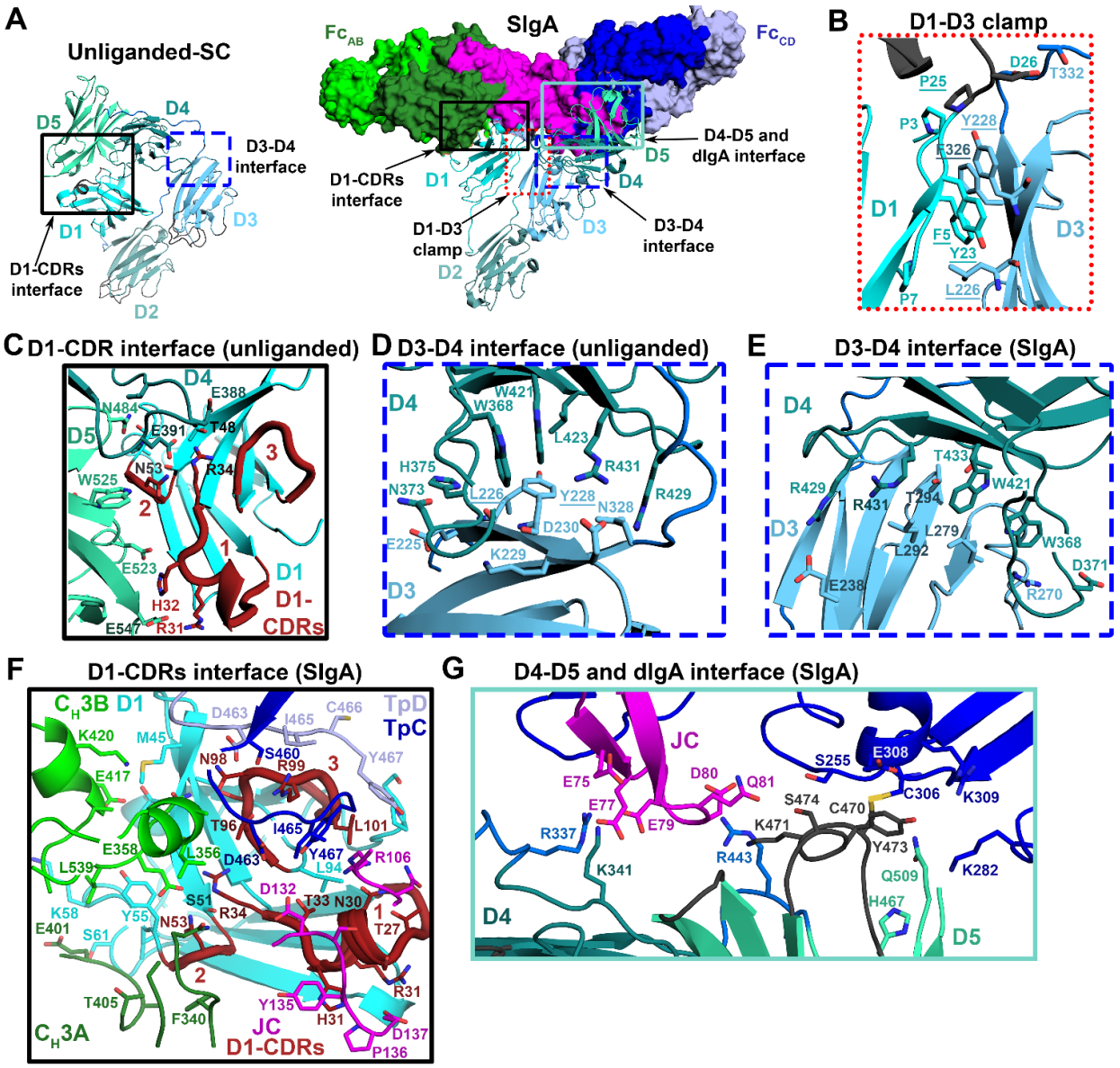

Supplemental Figure-1: Different interfaces of SC-domains in unliganded and liganded structures. (A) Homology model of unliganded mouse SC based on the unliganded human SC structure (PDB: 5D4K) and the mouse SIgA Cryo-EM structure (PDB: 7JG2). The SC is shown as a cartoon, with its five domains (D1-D5) colored different shades of cyan. In SIgA, dIgA components are shown as a molecular surface and colored as Fig. 1. The boxed regions are enlarged in B-G and detail residues engaged in molecular interactions for the (B) liganded SC D1-D3 clamp in SIgA, (C) unliganded SC D1 and D4-D5 interface, (D) unliganded D3 and D4 interface, (E) liganded D3 and D4 interface in SIgA, (F) liganded D1 and dIgA interface (G) the liganded D4-D5 and dIgA interface. In all panels, interfacing residues are shown as sticks. The D1-CDRs are shown as thicker loops denoted as 1, 2 and 3 corresponding to CDR1, CDR2 and CDR3 respectively, and they are colored brick red.

473

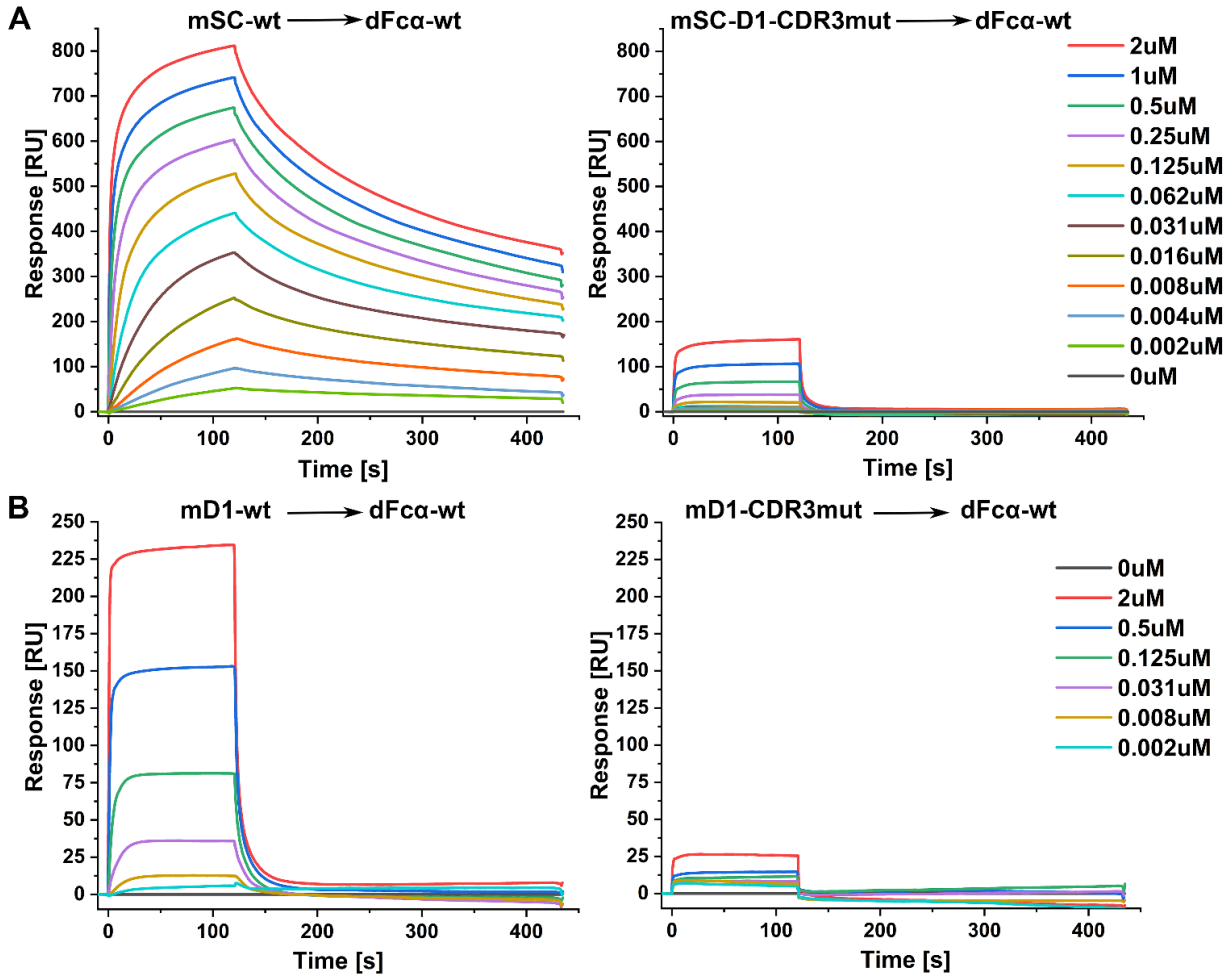

Supplemental Figure-2: mSC-wt and mSC-D1-CDR3mut binding to dFcα-wt at various concentrations (A) SPR sensorgrams showing the responses for the entire dilution series of mSC-wt and mSC-D1-CDR3mut binding to dFcα-wt, shown with the same scale. (B) SPR sensorgrams showing the responses for the entire dilution series of mD1-wt and mD1-CDR3mut binding to dFcα-wt. The responses for each analyte dilution are colored according to the keys (right), shown with the same scale.

474

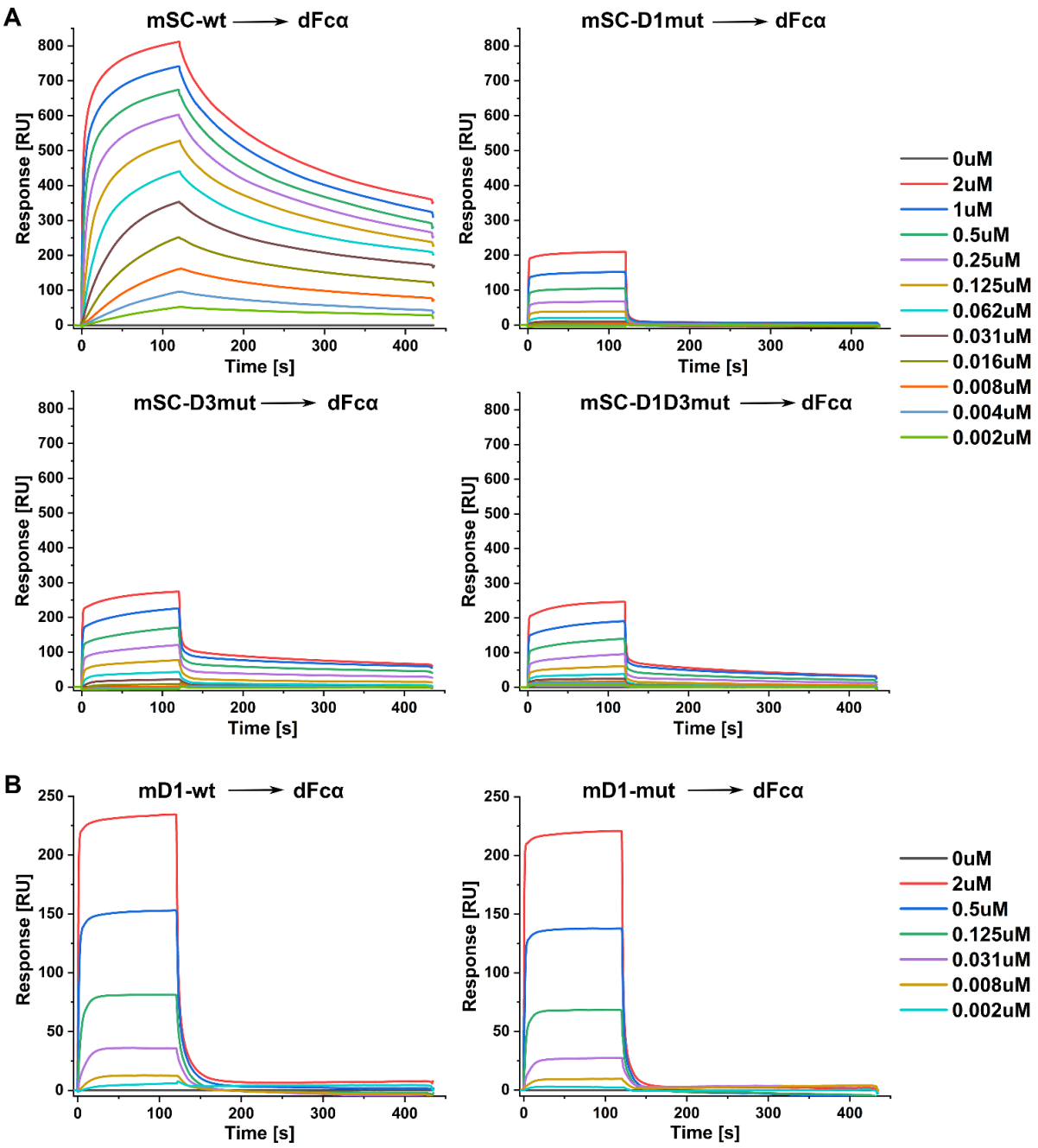

Supplemental Figure-3: Role of D1-D3 in binding stabilization and conformation change. (A) SPR sensorgrams showing the responses for the entire dilution series of mSC-wt, mSC-D1mut, mSC-D3mut and mSC-D1-D3mut, binding to dFcα-wt (2-fold dilution series starting from 2uM). All shown in same scale for comparison. (B) SPR sensorgrams showing the responses for the entire dilution series of mD1-wt, and mD1mut, binding to dFcα-wt (4-fold dilution series from 2uM). The responses for each analyte dilution are colored according to the keys (right).

Supplemental Figure-4.

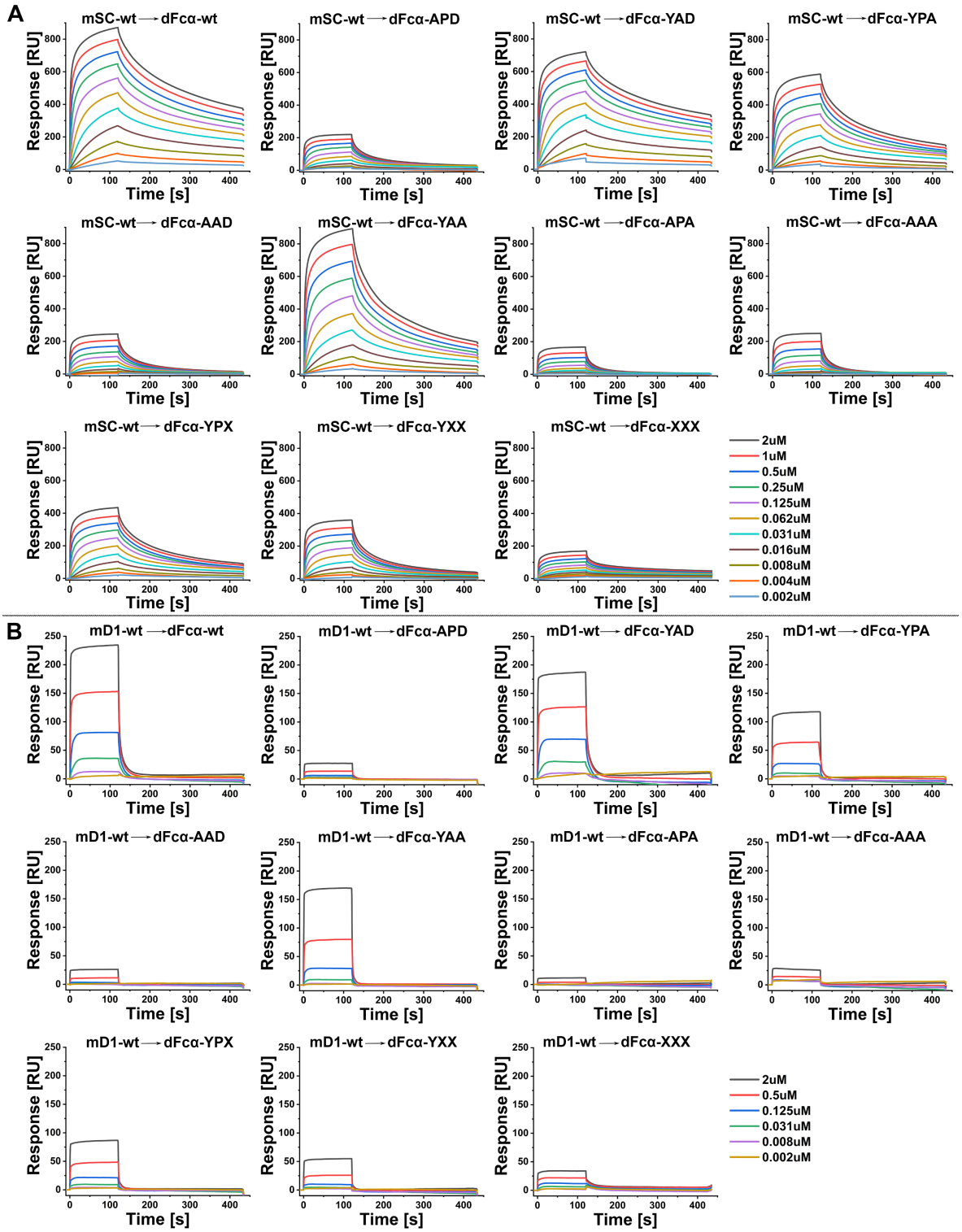

Supplemental Figure-4: (A) SPR sensorgrams showing the responses for the entire dilution series of mSC-wt binding to the indicated dFcα variants (shown on the same scales). (B) SPR sensorgrams showing the responses for the entire dilution series of mD1-wt binding to the indicated dFcα variants (shown on the same scales). The responses for each analyte dilution are colored according to the keys (right).